

HENRY

Hydraulic Engineering Repository

Ein Service der Bundesanstalt für Wasserbau

Article, Published Version

Schlesier, Hauke; Häfen, Hajo von; Goseberg, Nils
Physical modelling of tsunami barrier and debris interaction

Journal of Coastal and Hydraulic Structures

Verfügbar unter/Available at: <https://hdl.handle.net/20.500.11970/107571>

Vorgeschlagene Zitierweise/Suggested citation:

Schlesier, Hauke; Häfen, Hajo von; Goseberg, Nils (2021): Physical modelling of tsunami barrier and debris interaction. In: Journal of Coastal and Hydraulic Structures 1. <https://doi.org/10.48438/jchs.2021.0003>.

Standardnutzungsbedingungen/Terms of Use:

Die Dokumente in HENRY stehen unter der Creative Commons Lizenz CC BY 4.0, sofern keine abweichenden Nutzungsbedingungen getroffen wurden. Damit ist sowohl die kommerzielle Nutzung als auch das Teilen, die Weiterbearbeitung und Speicherung erlaubt. Das Verwenden und das Bearbeiten stehen unter der Bedingung der Namensnennung. Im Einzelfall kann eine restriktivere Lizenz gelten; dann gelten abweichend von den obigen Nutzungsbedingungen die in der dort genannten Lizenz gewährten Nutzungsrechte.

Documents in HENRY are made available under the Creative Commons License CC BY 4.0, if no other license is applicable. Under CC BY 4.0 commercial use and sharing, remixing, transforming, and building upon the material of the work is permitted. In some cases a different, more restrictive license may apply; if applicable the terms of the restrictive license will be binding.



Physical modelling of tsunami barrier and debris interaction

Hauke Schlesier¹, Hajo von Häfen², Nils Goseberg^{3,4}

Abstract

Tsunami events frequently cause vast damage to infrastructure and claim many human lives. A self-lifting membrane barrier was proposed to obstruct the impacts of tsunami while allowing permanent access to the sea while stored. Many aspects of this novel barrier concept have not been studied yet, including its performance under debris impact. Hence, this study firstly investigates the interaction between a self-lifting membrane barrier and tsunami-induced debris transport. A unique set of laboratory experiments in a wave flume are carried out, in which 20 ft shipping container models are washed into a membrane barrier by tsunami-like waves. Varying hydrodynamic conditions and an altered amount of debris is used to evaluate different magnitudes of surge and debris loading. This unique set of tests showed that the larger the amount of debris the stronger the surge propagation upstream the barrier decreases. The dynamic character of the barrier-debris-interaction prevented formation of a temporally stable debris dam. In total, 90% of debris transport further inland is obstructed by the membrane barrier. The barrier retains functionality under debris-loaded surge impact.

Keywords

Tsunami Barrier, Tsunami Debris, Self-lifting Membrane Barrier, Coastal Protection, Debris Damming, Hazard Mitigation

1 Introduction

On March 11, 2011, an earthquake with the intensity of 9.0 on the Richter scale shook the floor in 130 km distance to the north-east coast of Japan. Following the earthquake, a strong tsunami and its devastating impact particularly hit the prefectures of Iwate, Miyagi and Fukushima. As a consequence, the earthquake and tsunami damaged over 250,000 buildings, destroyed 140,000 of them completely and claimed almost 20,000 human lives (Dunbar et al. 2011; Fraser et al. 2013; Harbitz et al. 2016). Likewise, the tsunami event in the Indian Ocean 2004 and the recent one in Indonesia in September 2018 show, that despite their scarcity such events must not be underestimated (Shibayama 2015; Widiyanto et al. 2019).


Besides soft countermeasures such as tsunami evacuation, structural tsunami prevention measures remain to play an important role for tsunami hazard mitigation and are frequently considered by coastal planning agencies. Coastal dikes, sea walls and breakwaters are frequent among the common tsunami protection structures (Strusińska-Correia 2017; Shuto and Fujima 2009). Additionally, the mitigating effect of coastal forests as well as mangroves attracted notable attention as these vegetated coastal protection elements seemed to limit the damage to areas during the Indian Ocean tsunami in

¹h.schlesier@tu-braunschweig.de, Technische Universität Braunschweig, Germany
²h.von-haefen@tu-braunschweig.de, Technische Universität Braunschweig, Germany
³n.goseberg@tu-braunschweig.de, Technische Universität Braunschweig, Germany
⁴goseberg@fzk.uni-hannover.de, CoastalResearch Center, Joint Research Facility of Leibniz Universität Hannover and Technische Universität Braunschweig, Hannover, Germany

This paper was submitted on 4 January 2021. It was accepted after double-blind review on 31 May 2021 and published online on 17 June 2021

DOI: <https://doi.org/10.48438/JCHS.2021.0003>

Cite as: "Schlesier, H. G., von Häfen, H., & Goseberg, N. (2021). Physical modelling of tsunami barrier and debris interaction. Journal of Coastal and Hydraulic Structures, 1. <https://doi.org/10.48438/jchs.2021.0003> "

The Journal of Coastal and Hydraulic Structures is a community-based, free, and open access journal for the dissemination of high-quality knowledge on the engineering science of coastal and hydraulic structures. This paper has been written and reviewed with care. However, the authors and the journal do not accept any liability which might arise from use of its contents. Copyright ©2021 by the authors. This journal paper is published under a CC-BY-4.0 license, which allows anyone to redistribute, mix and adapt, as long as credit is given to the authors. 

2004 (Danielsen et al. 2005; Tanaka et al. 2007; Tanaka 2009; Tomiczek et al. 2020). Similar observations were made during the Tohoku tsunami in Japan 2011, which led to the design of forested embankments and comparable land use planning (Strusińska-Correia 2017). The use of such nature-based approaches to inundation mitigation is limited by the required space in inland direction, which is restricted in some coastal areas. For example, Lawrence and Nandasena (2019) showed that forest extending 150 m landwards had no mitigation effect on tsunami inundation.

Investigations in the aftermath of the Tohoku tsunami indicate that coastal structures could only provide a limited mitigation effect. Failures of sea walls, breakwaters and concrete revetments due to overflowing of water resulting in fracture of crown armor, overturning due to the force exerted by withdrawn water and scouring of the dike toe was observed (Kato et al. 2012; Fraser et al. 2013). It should be noted that not all structures were designed for tsunami loadings but for floods, typhoons or wind waves. Overall, breakwaters with a combined length of 8,500 m collapsed during the Tohoku tsunami event (Fraser et al. 2013). Therefore, Takahashi et al. (2011) suggested that emphasis should be placed on stability so that protection infrastructure stays structurally intact even during high impact tsunami.

1.1 Self-lifting membrane barrier

Coastal structures tend to compete for space and aesthetics within the coastal area while also impacting local ecosystems. The constraints that are attached to these various considerations resulted in an increasing effort to design and conceptualize new tsunami barriers (see Marissen et al. 2013; Kimura et al. 2014; Chandramouli et al. 2018). The presently debated concept of tsunami barriers assumes them to remain hidden in a dormant storage provision until a tsunami event’s associated flow reaches the barrier’s location; only in such an event, the barrier is activated and may self-lift through appropriate design features, e.g., floatation devices that hold the upper vertical member of the barrier afloat with the incoming waters. A very first example of that defense strategy was suggested by Marissen et al. (2013) who proposed a membrane barrier which is stored folded to minimize space requirement and lifts itself due to buoyancy forces on a floating member (FM, see Fig. 1). The onshore located barrier could be led along the shore to protect a specific coastal area or bay. A construction of a few kilometers could be installed at cities and power plants or downstream of a harbor area (Marissen et al. 2013). The flexible membrane could be made off an Ultra-High-Molecular-Weight-Polyethylene (UHMWPE) fiber with a tensile strength of 3.4 kN/mm to withstand the hydrostatic and hydrodynamic forces acting on the barrier (Marissen 2011; Marissen et al. 2013). The bottom end of the membrane would be anchored to the soil, while the upper end is connected to the FM. The FM itself is connected to an upstream anchored UHMWPE fiber cable (see Fig. 1). Marissen et al. (2013) calculated, that a 3 mm thick membrane could take up hydrostatic forces of a 20 m high flood. The UHMWPE fiber has a density of 975 kg/m³, hence it would float (Marissen 2011).

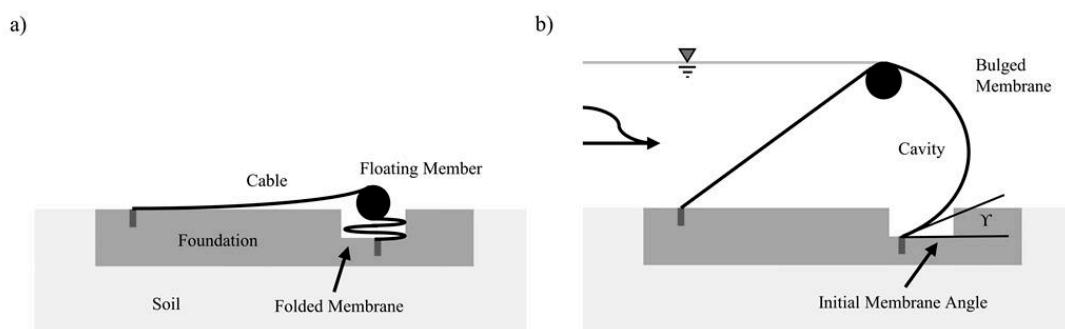


Figure 1: Schematic depiction of a self-lifting membrane barrier after Marissen et al. (2013); (a) stored and (b) lifted.

Marissen et al. (2013) suggested first basic design guidelines based on hydrostatic considerations:

- Initial membrane angle γ (Fig. 1b) should be smaller than 22.9° to reduce tension forces on the membrane and horizontal forces on the cables.
- Membrane contour length should be more than double the design water depth.
- Horizontal distance between FM and cable anchorage should be at least one and a half times the design water depth.

Marissen et al. (2013) proposed design guidelines based on the pressure distribution along the membrane in a hydrostatic equilibrium state. However, this is a highly simplified scenario since kinetic energy of the impacting tsunami wave will lead to different pressure distributions and overall higher pressure. Moreover, membrane and cable forces are in a dynamic balance during tsunami loading leading to various parameters being design relevant. Thus, barrier parameters likely need to be altered when hydrodynamic forces are considered. Hofland et al. (2015) investigated the dynamic behavior of the barrier in a 1:100 scaled model (Hofland et al. 2015) and found that the principle of the self-lifting membrane barrier (SLMB) is basically applicable. For flow depths larger than the barrier height the barrier stayed lifted, even while overflow occurred. It is still unclear if the barrier is susceptible to other failure mechanisms such as extensive scouring or abrasion of cables and membrane due to debris. Hofland et al. (2015) noted that a huge lack of knowledge concerning design and behavior of the barrier exists. Understanding local and irregular load concentrations, foundation loading, barrier side end design, varying wave parameters and debris impact would need more research. Concerning debris impact, Hofland et al. (2015) hypothesized that most debris impact would be stopped by the barrier. Furthermore, the acceptance among the local population of constructing such a barrier over multiple kilometers remains to be answered.

1.2 Interactions between tsunami, structures, and debris

Past tsunami events showed that debris such as trees, cars, boats, poles, and containers can cause immense damage (EERI 2011; Fraser et al. 2013; Palermo et al. 2013). The debris entrained in tsunami flood waves cannot be confused with debris flows (alpine/mountainous conditions) where –unlike to process at hand– an intricate mass and force balance between soil, pore pressure and free surface water flow exists. Various studies, both physical and numerical, have been conducted; multiple approaches have been considered to estimate debris impact forces generated by objects that are propagated by surges, bores and broken solitary waves (see Haehnel and Daly 2004; Nouri et al. 2010; FEMA 2012; Paczkowski et al. 2012; Como and Mahmoud 2013; Ko et al. 2015; ASCE 2016; ROH 2018). On the other hand, Nistor et al. (2017a) emphasized the importance of understanding tsunami-driven debris transport for better evaluating the hazard risk for a structure by also considering the likelihood of debris impact.

Naito et al. (2014) developed a model to estimate potential debris distribution areas, distances and spreading angles based on satellite images made of shipping container terminals before and after the Tohoku tsunami event in 2011. Nistor et al. (2017b) investigated tsunami-driven debris transport over a horizontal apron under laboratory conditions. They found that the maximum longitudinal displacement as well as the spreading angles depends on the amount of debris. Goseberg et al. (2016b) showed by accurately measuring the debris' path (Goseberg et al. 2016a) that obstructions have an influence on the spreading angle. It was shown that a first row of obstructions decreases the maximum longitudinal transport of debris. Stolle et al. (2018a) tested an approach where the final position of displaced debris can be described by a probability-density-function (PDF), allowing to predict the likelihood of debris impact. It was also found that standard deviation of the debris position distribution depends on initial debris orientation. Yao et al. (2014) investigated motion of debris accelerated onto a sloped beach model by a broken solitary wave in laboratory. They concluded that presence of debris can reduce maximum inundation (although measurement of maximum inundation was subject to high uncertainty). A similar effect on maximum inundation was observed due to presence of built environment (Goseberg and Schlurmann 2015). This supported Khan et al. (2000) who observed an increase in surge deceleration and surge height with increasing debris amount. Yao et al. 2014 underlined the high uncertainty concerning debris position and maximum inundation. In conclusion, Stolle et al. (2018a), Nistor et al. (2017a), Goseberg et al. (2016a) and Yao et al. (2014) support the finding of Matsutomi (2009) that tsunami debris transport is characterized by a high degree of randomness.

Laboratory conditions should approximate the complexity associated with the spatiotemporal scales of the fluid-structure-interaction. Thus, tsunami propagation over land is often simulated by bores or surges using dam-break waves. It has been shown that flow parameters of dam-break-waves are in reasonable agreement with tsunami field data (Chanson 2006, Nistor et al. 2009). Several analytical solutions for surges and bores have been established (Ritter 1892; Whitham 1955; Chanson 2005). Hence, many studies used dam-break waves to investigate interactions between onshore propagating tsunami, debris, and structures (Khan et al. 2000; Nouri et al. 2010; Shafiei et al. 2016; Nistor et al. 2017a; Derschum et al. 2017). Multiple shapes, sizes, and masses of debris models have been used to represent different kinds of debris like large woody objects (Nouri et al. 2010), houses (Yao et al. 2014; Ardianti et al. 2018), and shipping containers (Ko et al. 2015; Nistor et al. 2017a; Derschum et al. 2017; Stolle et al. 2017a). Especially debris representing 20 ft shipping containers were commonly used due to their simple geometry and widespread existence in tsunami-prone

areas world-wide. Many studies concentrate on one type of debris (Cheng Chen et al. 2020; Derschum et al. 2017; Häfen et al. 2021; Khan et al. 2000; Nouri et al. 2010; Shafiei et al. 2016; Yao et al. 2014; Nistor et al. 2017a).

In contrast to the above outlined research on debris transport in the coastal zone, little research has been attributed to investigate the ability of tsunami barriers to block debris. Pasha and Tanaka (2016) carried out experiments to investigate tsunami debris capturing potential of finite-length inland forest. Umeda et al. (2018) investigated debris interaction on an onshore located perforated tsunami barrier but focused on the inundation mitigation effect and the debris impact force exerted on the barrier. Shao (2005) and Takagi and Bricker (2014) used numerical models to investigate mitigation effects of breakwaters. Stolle et al. (2017b) experimentally investigated loads and effects associated with debris damming. In their experiment, debris with various geometries were blocked by an obstacle under steady-state flow. This resulted in an agglomeration of debris in front of the obstacle and subsequently increasing the load on it (Stolle et al. 2017b). In another study Stolle et al. (2018b) investigated debris damming loads under transient supercritical flow conditions and found that debris dams are less stable than under steady-state flow conditions. Usually, the phenomenon of debris damming is observed beneath bridges where wooden logs accumulate and eventually block the flow. Robertson et al. (2007) described debris damming as a phenomenon, where debris become wedged at a structure, resulting in increased drag and inertia forces due to a disrupted flow field. Schmocker and Hager (2011) noted a backwater rise caused by debris damming, potentially leading to overflow of the structure. Melville and Dongol (1992) as well as Pagliara and Carnacina (2013) showed that debris damming can lead to increased scouring.

1.3 Objectives

Tsunami and their severe effects in coastal areas hold immense potential for destruction of buildings, structures, and may inflict human live losses. Tsunami-induced debris and debris-related loading scenarios are research topics that require continues effort. Beside knowledge gaps related to structural loadings, it remains vital to continue research on novel approaches regarding protection measures such as tsunami barriers that can act as an element in a tsunami defense system. Little research exists concerning the behavior and potential of tsunami-barriers and their interaction with debris. This study firstly shed light onto the applicability of a SLMB under debris loading. The specific objectives of this study are:

- To evaluate the effect of debris on flow parameters such as flow depth and propagation velocity and consequences for barrier functionality.
- To investigate the potentiality of debris-induced damming upstream of the barrier under transient flow conditions.
- To analyze the performance of the barrier to mitigate debris transport.

As this preliminary study primes for extensive investigations, the parameter space is limited. The study focuses on a commonly utilized type of tsunami debris and a limited variation of wave conditions. Although understanding hydrodynamic and debris forces exerted on the barrier and cables is vital when it comes to application, the quantification of these forces is outside the scope of this study.

2 Methodology

2.1 Test facility

The set of experiments is conducted in a wave flume at the Leichtweiß-Institute for Hydraulic Engineering and Water Resources, Department of Hydromechanics and Coastal Engineering at Technische Universität Braunschweig, Germany. The wave flume has a length of 19 m, a width of 0.30 m, and a depth of 0.35 m (Fig. 2). A dam-break gate separates a 10.87 m long propagation section from a reservoir section with a length of 8.13 m. To simulate tsunami beach run-up, a sloping beach is made of wooden board (marine plywood, smooth surface on top), which measures 6.60 m in length and 0.33 m in height resulting a 1:20 slope which lies in the range of naturally occurring beach slope angles (Pethick 1984). A horizontal section spans 4.27 m from the dam-break gate to the toe of the slope (Fig. 2). Flume bed and walls are made of acrylic glass.

Surges were generated by application of the dam-break method. The dam-break gate is made of a metal plate and placed between two boards with vertical slots allowing for a rapid vertical lifting of the plate, thereby releasing the water impounded in the reservoir. Rubber stripes connected to the metal plate edges are used to seal the gate. The Hager-Lauber gate opening criterion is applied, which is rather conservative (von Häfen et al. 2019), to ensure a dam-break wave being unaffected by the gate opening process. According to Lauber and Hager (1998), gate opening needs to be shorter than the time t_{op} :

$$t_{op} \leq \sqrt{\frac{2h_0}{g}} \tag{1}$$

where h_0 is the impoundment depth and g the acceleration of gravity.

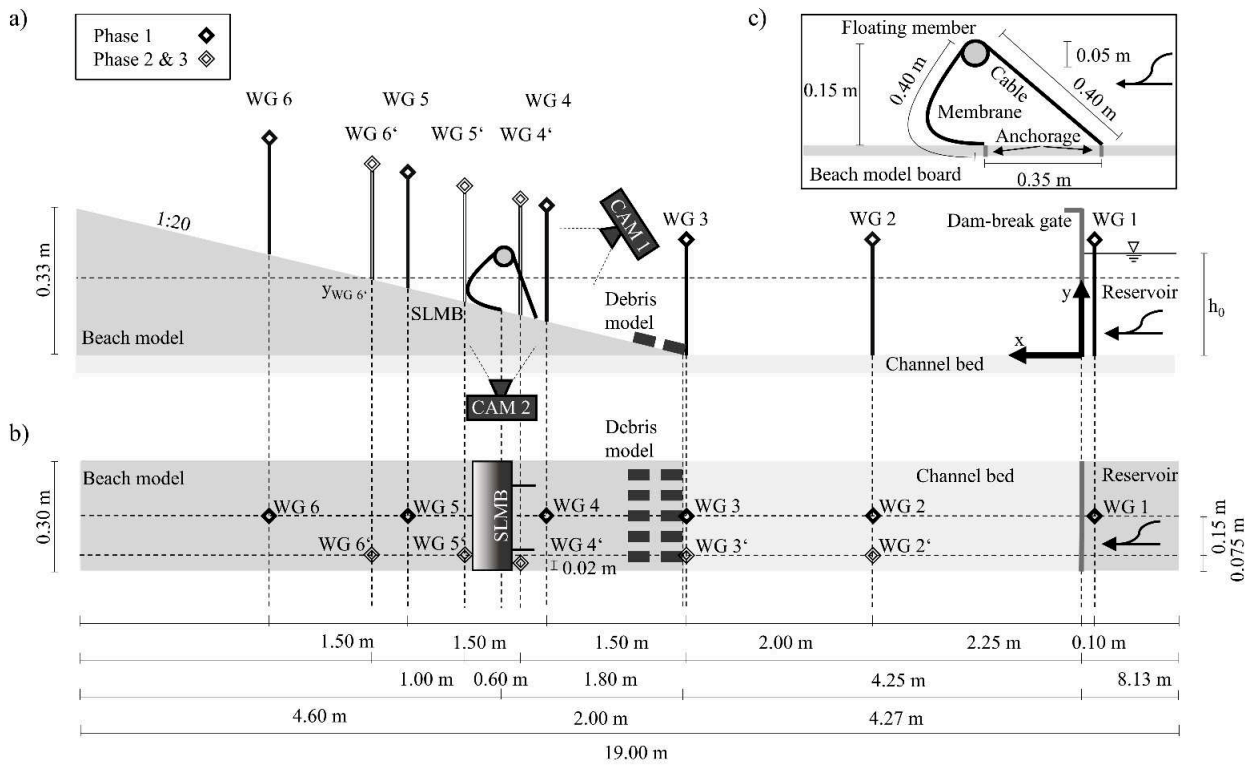


Figure 2: Flume dimensions and bathymetry of the test facility as well as the Self-Lifting Membrane Barrier (SLMB) and measuring devices: Wave Gauges (WG), Cameras (CAM) and their positions within the three phases of the experimental protocol. a) side view, b) top view, c) detail of the lifted SLMB including dimensions. Wave gauge positions indicated without index ‘ (e.g., WG 5) belong to experimental phase 1. The gauge positions are shifted for experimental phase 2 & 3 indicated by index ‘ (e.g., WG 5’, see section 2.2).

The opening time is assessed via video analysis and observed to be $0.179^{+0.017}_{-0.033}$ s. Thus, it remains smaller than the maximum opening time of 0.226 s as per the Hager-Lauber-Criterion (Lauber and Hager 1998) for even the lowest impoundment depth.

Hence, the generated dam-break waves are in good agreement with analytical solutions: Correlation coefficients r for observed surge profiles and the Ritter solution are in the range of 0.9841 to 0.9903 (Ritter 1892) and for observed surge propagation between 0.9993 to 0.9999 compared to the Chanson solution with a friction factor of 0.012 (Chanson 2006).

To ensure comparable flow conditions in model and prototype scale, Froude similitude is applied. Derived from experiments by Hofland et al. (2015), a length scale of 1:100 is chosen. Flow depths observed roughly 6 m downstream of the dam-break gate are in the range of 0.13 m to 0.17 m (Fig. 5a, b) and therefore represent a surge of 13 m to 17 m in prototype scale. Such flow depths represent large tsunami events and thus compare well to flow depths in nature (EERI 2011). The observed surge propagation velocity at the toe of the beach model is in a range of 1.25 m/s to 1.5 m/s (Fig. 5c, d), resulting in velocity of 12.5 m/s to 15 m/s in prototype scale. Similar velocities were observed during past tsunami events (Kawata et al. 1999; Morton et al. 2007; Choowong et al. 2008).

Due to their wide application in previous studies and their simple geometry, 20 ft shipping containers are used as debris. External dimensions of 20 ft containers are 6.058 m in length, 2.428 m in width and a height of 2.591 m. Empty containers of this size typically weigh 2250 kg and can reach 32,500 kg under maximum payload conditions (Norm ISO 668:2013(E)). In 1:100 scale, a container has a size of $0.06 \times 0.024 \times 0.024 \text{ m}^3$. The mass of the floating wooden container models is 0.028 kg resulting in a density of 810 kg/m^3 . Such a mass would represent a container with 79% payload. Table 1 contains the debris' parameters in prototype and model scale.

Table 1: Debris parameters of 20 ft shipping containers in prototype and model scale.

Scale	Length [m]	Width [m]	Height [m]
Prototype	6.058	2.428	2.591
Model	0.060	0.024	0.024

A SLMB in 1:100 scale is modeled (see Fig. 2c) to test its performance with respect to tsunami inundation and debris retention. To determine the membrane contour and cable length, the preliminary design recommendations of Marissen et al. (2013) were employed (design water depth was set to 0.15 m) both to have initial guidance and to ensure latter comparisons. This results in a length of 0.40 m for both the membrane contour and cable. Model membrane and cables are made of polyethylene. The triple-welded membrane fabric has a specific weight of 0.14 kg/m^2 and a tensile strength of 150 N/cm (for explanations of scaling of tensile strength see section 3.5). On both edges of the membrane, a 0.01 m wide and 0.32 m long stripe of tape is added to reduce side leakage between membrane and flume wall. Due to the water pressure acting on the membrane and unfolding it entirely, the tape is pushed against the acrylic side walls of the flume sealing the membrane against the flume wall. However, the sealing is not fully watertight which may have resulted in a minor model effect discussed in section 3.5. A FM made from a PVC pipe with sealed ends of acrylic glass is connected to the upper part of the membrane. The FM has a diameter of 0.05 m and generates a maximum of roughly 6 N of buoyancy in model scale. Two cables are connected to the FM which is anchored to the beach model; so is the bottom part of the membrane (see Fig. 2c). The parameters of the SLMB are listed in Table 2.

Table 2: Dimensions and properties of the SLMB model.

Parameter	Unit	Value
Membrane width	[m]	0.30
Membrane thickness	[mm]	0.40
Membrane contour length	[m]	0.40
Floating member diameter	[m]	0.05
Floating member width	[m]	0.30
Cable length	[m]	0.40
Max. float buoyancy	[N]	6

2.2 Experiment Protocol

The experimental protocol includes a total of 24 experiment runs within three different experiment setups (Table 3). Different amounts of debris models D are used in each experiment run to simulate a varying degree of debris loading. A number of 10 pieces of debris represents a low debris loading, while a total amount of 25 pieces is a high loading. Debris models are placed in rows of five pieces at the toe of the sloping beach (Fig. 2b). The longitudinal and lateral distance from one piece of debris to another is 0.024 m. The debris are orientated with their long side parallel to the flow direction and care was taken to accurately position the debris prior to each experimental run. In order to position debris accurately tags were marked to the according places on the beach model board.

All experimental runs are carried out with two different initial impoundment depths, which allows the generation of surges with varying flow depths and propagation velocities; these results in a variation of the surge impact intensity on the SLMB and debris, respectively. For this study, an impoundment depth of 0.25 m for a low surge impact case and 0.30 m for a high surge impact case is used. This results in flow depths at barrier position lower than the barrier design water depth in the low surge impact case and higher than barrier design water depth in the high surge impact case. Every experimental configuration is repeated three times. Video analysis reveals that in some of the runs FM clenching between flume walls occurred; these runs are omitted from the analysis as they result in excessive flow over the SLMB (e.g., exclusion of run 19). The remaining experiment runs are listed in Table 3, which contains the entire experiment protocol.

Table 3: Experiment protocol.

Phase	Test Nr.	Barrier	Debris amount D [-]	h_0 [m]
1	1, 2, 3	no	-	0.25
1	4, 5, 6	no	-	0.30
2	7, 8, 9	with	-	0.25
2	10, 11, 12	with	-	0.30
3	13, 14, 15	with	10	0.25
3	16, 17, 18	with	10	0.30
3	(19), 20, 21	with	25	0.25
3	22, 23, 24	with	25	0.30

Within the first phase (Table 3), reference data on surge flow depths and propagation velocities is collected. In this phase, the surge propagation is unobstructed by the barrier or debris. Wave gauge (WG) 2 is placed between dam-break gate and beach model to measure the surface elevation time history of the surge in the horizontal flume section. Wave gauges 3 to 6 are placed on the beach in increments of 1.50 m (Fig. 2a, b).

For the second and third experiment phase (Table 3) the barrier is implemented, located 6.27 m downstream of the dam-break gate (2 m downstream of the beach toe, see Fig. 2a, b). In this case, the barrier represents an onshore protection structure. At this position, maximum flow depths represent the barriers design water depth (see Fig. 5a, b). To refine surface elevation data measurements in the vicinity of the barrier, WG 4' and 5' are moved closer to the barrier. Downstream of the barrier, WG 5' and 6' can measure flow depths of overflowed water (see Fig. 2b). Data collected in phase two serves as reference for flow parameters observed in experiment runs for phase three in which debris models are added.

In the third phase, a varying amount of debris are placed at the toe of the beach model (see Fig. 2a, b). This simulates a multitude of containers stored in a harbor area. An incoming tsunami accelerates the debris downstream into the barrier. To reduce the risk of the debris impacting the wave gauges and thus being affected in their flow path, the wave gauges are shifted closer to the flume wall (see Fig. 2b).

2.3 Instrumentation and Synchronization

The instrumentation includes six wave gauges (AWP-24-2, capacity-type, see Table 4) and two cameras (CAM). The cameras (CAM 1, CAM 2) are installed in close proximity to the barrier. The field of view (FOV) of CAM 1 allows for an overview and upstream perspective on the barrier, whereas the FOV of CAM 2 provides a side view perspective (see Fig. 2a). Synchronization of camera footage was achieved visually by surge arrival at the tape markers upstream the SLMB (see Fig. 3a) as well as by a clapping noise on the soundtrack. An evaluation of the image data recorded allowed for qualitative and quantitative assessment of the surge-barrier-interaction, including debris damming and debris obstruction as well as capture ratios.

Wave gauges WG 2 to 6 are located at various positions (Section 2.2). The reference wave gauge WG 1 is located at a fixed position 0.1 m upstream of the dam-break gate (Fig. 2). Within this study, the instant of gate opening is defined as time zero. Time zero (t_0) is determined based on the surface elevation time history of WG 1, which detects a dropping water level once the gate is opened (t_1 , threshold $\Delta h = 0.03$ m). Since WG 1 is installed in 0.1 m distance to the gate, an offset between gate opening (t_0) and surface elevation drop (t_1) exists. This offset can be determined based on the velocity of the wave front propagating in the reservoir and the distance Δx_{g1} between gate and wave gauge: $t_0 = t_1 - \frac{\Delta x_{g1}}{\sqrt{gh_0}}$.

Table 4: Properties of utilized instrumentation.

Abbr.	Instr. Name	Manufacturer	Amount [-]	Meas. Unit	Sampl. Freq. [Hz]	Accuracy [%]	Resolution
WG	AWP-24-2	Akamina Technologies, Ottawa, Canada	6	Water Depth [m]	200	0.15	-
CAM	Everio GZ- HD40	JVC	2	-	50	-	1920x1080

3 Results

3.1 Influence of SLMB on hydrodynamics

A flow depth time history of (WG 4') is depicted in Fig. 3b to visualize the stages of the barriers dynamic response on the arrival of the surge front; this is a complex process that deserves further description. The SLMB is initially resting at the beach slope (Fig. 3a, photograph 1). In the first instants after the surge front arrival the SLMB is overflowed while simultaneously downstream pushing of the FM is observed (Fig. 3a photograph 2). Within the following approximately ten seconds surge flow depth increases first and then being constant (“Inundation”, see Fig. 3b). Then, the flow direction turns and retreating water from the beach slope interacts with the SLMB, now afloat and functioning as per its design (Fig. 3a photograph 3 & 4). The downward flow starts to form a hydraulic roller (Fig. 6). This results in an abrupt increase in flow depth (Fig. 3b, Fig. 6).

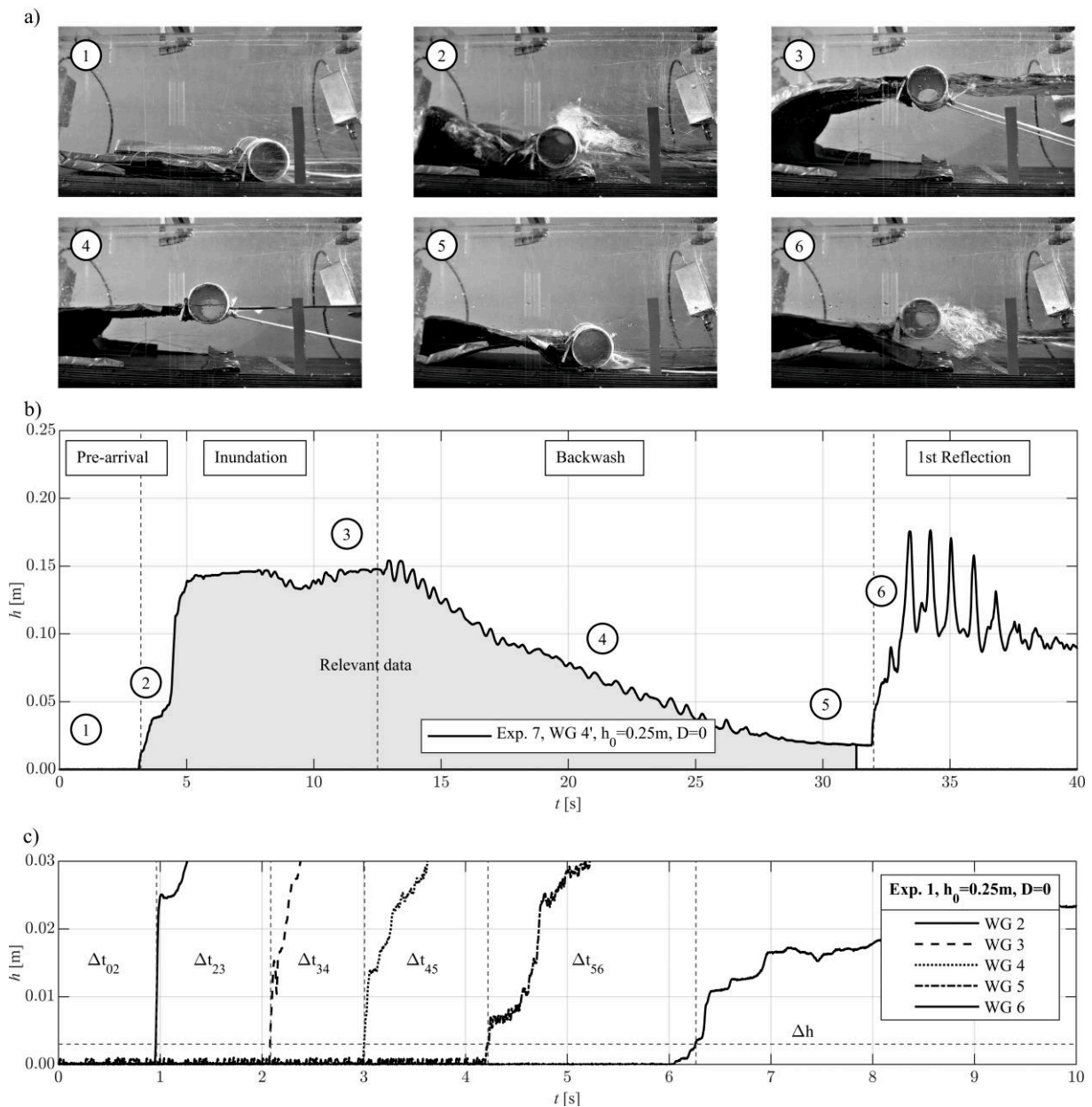


Figure 3: (a) Phases of the SLMB interacting with the approaching surge. (b) Surface elevation time history for WG 4', experiment 7, and references to associated phases of the barrier-surge-interaction shown in (a). (c) Determination of surge arrival times (Δt_{ij}) at different wave gauges, presented as a time history of flow depth. Vertical grey dashed lines indicate the estimated arrival times. Threshold is indicated by Δh (horizontal grey dashed line).

The roller moves upstream as a bore which is reflected multiple times at the flume wall and the beach model (“1st Reflection”, see Fig. 3b photograph 6). Even though tsunami waves may be reflected by landmasses or in bays (Yamazaki and Cheung 2011), within this study surge development is considered only from arrival to right before the first reflection.

Surge arrival times for WG 2 to 6 are depicted in Fig. 3c. The instant is detected with a threshold of $\Delta h = 0.002$ m in flow depth at each particular wave gauge (see Fig. 3c).

For estimating loadings on structures, the maximum flow depths and flow velocities (and their timing with respect to each other, Chock 2016) are important. Maximum flow depths can be derived from the surface elevation time histories by finding the maximum value within the relevant observation period (see Fig. 3b). Surge propagation velocities can be calculated by dividing the distance between two wave gauges (Fig. 2) by the corresponding difference in surge arrival time assessed through the method shown in Fig. 3c.

Prior to a more specific presentation of the debris capture efficiency of the SLMB, it is essential to provide a clear observation of the effect that the SLMB has on the run-up process as compared to an unprotected beach; that is a situation without a SLMB structure present. An illustration of the maximum surface elevations over the entire run-up/run-down sequence for runs with and without the SLMB are shown in Fig. 4. Runs without the SLMB present show a nearly constant gradient of maximum surface elevations in flume axis (x -direction, Fig. 4), both for impoundment depths of 0.25 m and 0.30 m. Hence, surface elevation is interpolated linearly between wave gauges and extrapolated beyond the last wave gauge. Linear interpolation has been used in former studies for minimum flow depths and maximum crests amplitudes of landslide-generated tsunami in laboratory (Jaffe and Gelfenbuam 2007; Lange et al. 2020).

For experiments where a SLMB is present, it is assumed that propagation velocity downstream of the barrier is quasi zero due to kinetic energy of the wave being dissipated with barrier overflow. In runs with high surge impact, WGs downstream the SLMB can provide insight on the effect of the barrier on run-up (Fig. 4b). It is observed that maximum surface elevation at WG 6’ are not surpassing maximum surface elevation at WG 5’, as it is expected if propagation downstream is governed by kinetic energy. In fact, Figure 4b shows that maximum surface elevation is roughly equal downstream of the SLMB. Hence, propagation velocities downstream the barrier are quasi zero too (Fig. 5c and d). The extrapolation and interpolation of maximum surface elevations for runs with and without barrier are discussed in Section 4.

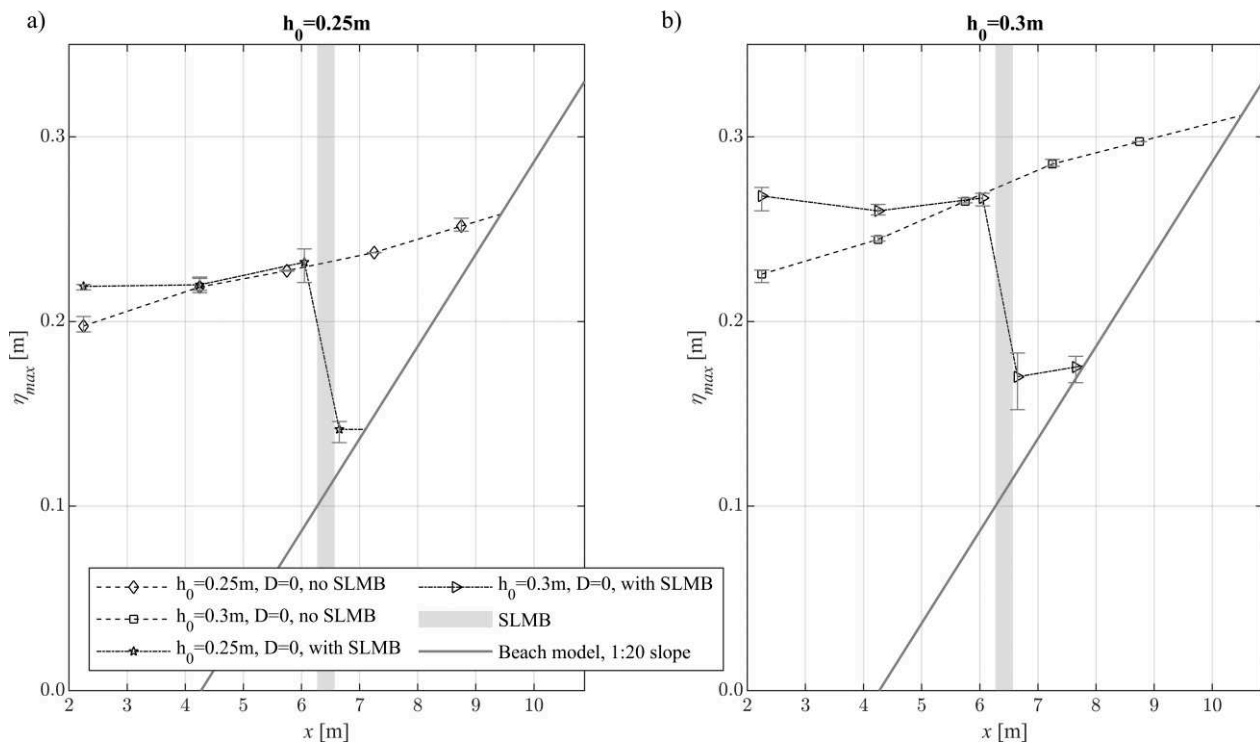


Figure 4: Averaged maximum surface elevations for runs with and without a SLMB present for (a): low and (b): high impoundment depth. Error bars show minima and maxima within repetitions. Extrapolation for runs without barrier is linear due to the approximately constant gradient of maximum surface elevation. Extrapolation for runs with barrier is applicable since propagation velocity downstream the barrier is quasi zero.

3.2 Debris effect on wave parameters

The SLMB needs to be functional under debris loading. Thus, understanding the effect of debris on wave parameters is crucial for estimating changes in hydrostatic and hydrodynamic forces exerted on the barrier in debris versus non-debris loading cases. Fig. 5 shows the effect of debris on maximum flow depths and surge propagation velocities for different impoundment depths and debris amounts. An effect of debris on maximum flow depth upstream the barrier cannot be observed (see Fig. 5a, b). In runs with low surge impact, the maximum flow depths downstream the barrier increase with increased debris amount, however no such effect is observed for runs with high surge impact. Presence of the barrier leads to decreased maximum flow depths downstream and increased maximum flow depths upstream the barrier (Fig. 5a, b).

The effect of debris amount and barrier on surge propagation velocity is shown in Fig. 5c, d. An increased debris amount leads to slightly decreased upstream surge propagation velocities in barrier proximity. This effect is more pronounced in runs with low impoundment depth. However, the effect of debris on downstream surge propagation velocities is unclear: In the high surge impact scenario, downstream propagation velocities vary greatly with debris amount, however no effect can be observed in the low surge impact scenario.

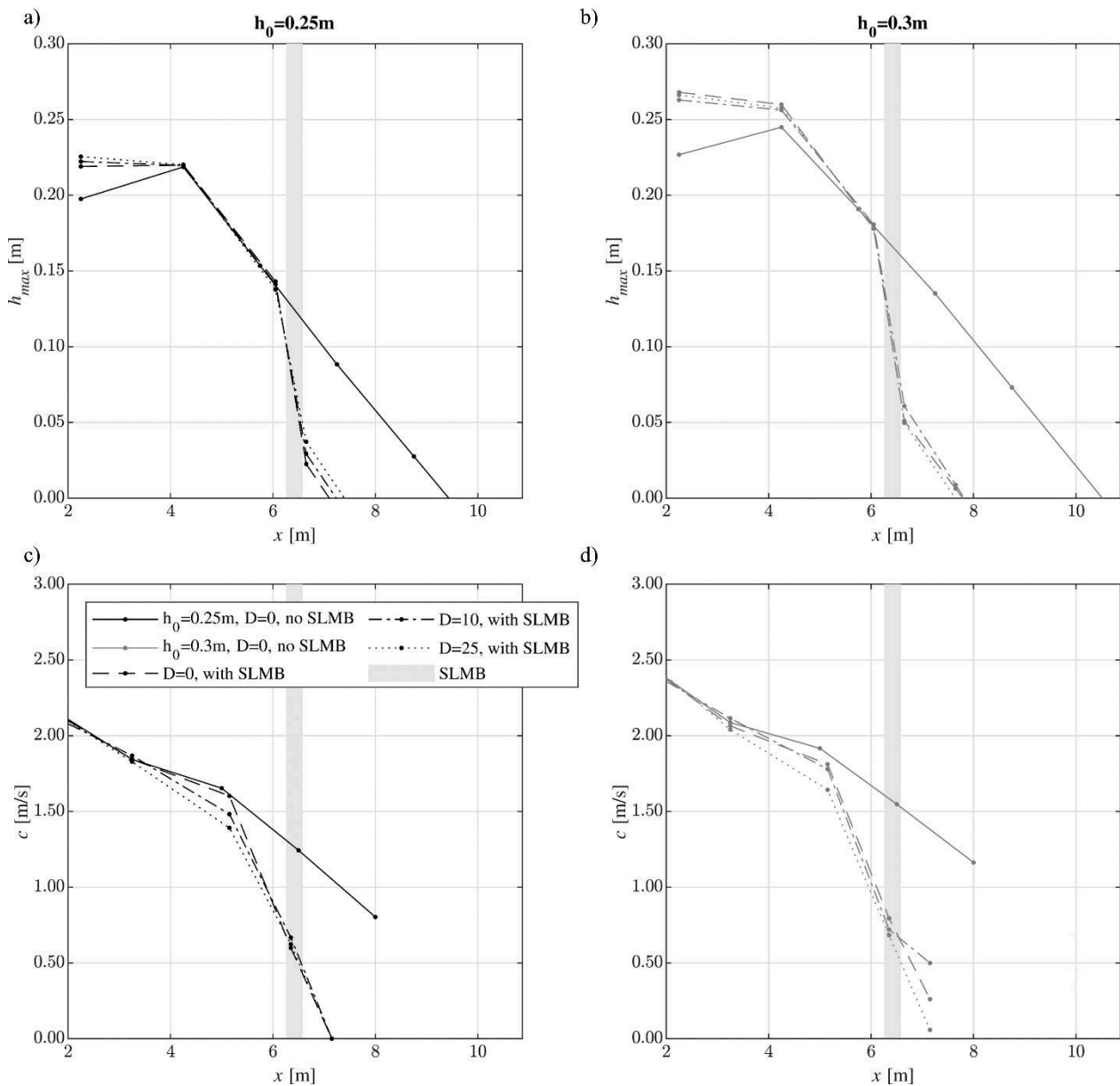


Figure 5: (a), (b) Debris effect on maximum flow depths. (c), (d) Debris effect on surge propagation velocity. Plotted are the mean values of respective runs (see Table 3).

Debris, present in the flow approaching a shoreline or propagating on shore, may contribute to an increased water level in the vicinity of barrier-like topographies. A closer look needs to be taken in the context of SLMB to evaluate the possibilities of that debris-induced backwater rise. To that end, mean flow depth time histories at WG 4' for various debris amounts and impoundment depths are shown in Fig. 6. A slight delay of surge arrivals with increased debris amount is observed, which is congruent with the results shown in Fig. 5c, d. In the high surge impact case increased debris amount leads to slightly higher flow depths at the beginning of the roller formation. Both Fig. 5a and 6 indicate that debris-induced backwater rise does not lead to increased maximum flow depths.

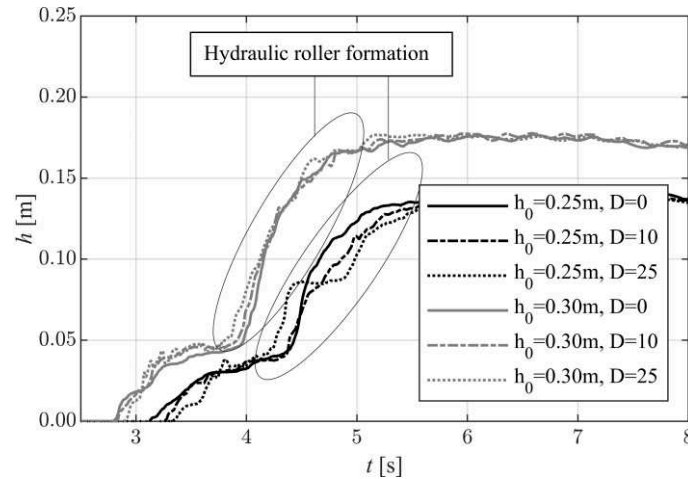


Figure 6: Debris effect on mean flow depth time histories upstream of the barrier for various debris amounts. Ellipses indicate the hydraulic roller formation.

3.3 Barrier-Debris-Interaction

The phenomenon of backwater rise is usually attributed to debris damming (Stolle et al. 2018b). Image data is used to observe debris dam formation during the barrier-debris-interaction. Fig. 7 depicts different stages of interaction, shows the barrier as well as the debris dynamics, and assigns overtopping events to interaction stages. These stages are defined as follows:

- The surge arrives at the FM followed by debris models. Impacting surge and debris exert horizontal forces on the FM pushing it in downstream direction (Fig. 7 box a). Hence, this stage is called the *push-back stage*. Debris are pushed against the FM, resulting in debris dam formation upstream the SLMB. Few debris models overtop the barrier during this early stage. In total, only 11.1% (2 out of 18) of all overtopping events occur during this $0.68^{+0.19}_{-0.15}$ s long *push-back stage* (Fig. 7).
- Then, cable forces prevent the FM of being pushed back further (Fig. 7 box b). Buoyancy forces on the FM become dominant and the barrier lifts up (*lifting stage*). A cavity between beach floor and membrane opens (compare Fig. 1b, Fig. 7 box b). Water rushes in, leading to some debris entering the cavity. Then, flow changes direction rapidly pulling captured debris back upstream (Fig. 7 box b). This results in disintegration of debris dam into a loosely agglomerated field of debris upstream the FM, creating a ‘debris carpet’ (Stolle et al. 2017b). The lifting stage lasts for $0.48^{+0.19}_{-0.22}$ s and accounts for one third (6 out of 18) of overtopping events (Fig. 7).
- Lifting of the structure stops when cable, membrane, and FM forces are in an *equilibrium state* and the SLMB stabilizes (Fig. 7 box c). Now, the SLMB is in its design state of operation. Barrier overflow and debris overtopping might occur. Overtopping events during equilibrium state account with 55,6% (10 out of 18) for most overtopping events. However, all overtopping events in equilibrium state occur in runs with high impoundment depth.

Barrier-debris-interaction is a highly dynamic and transient phenomenon. Usually, only $1.15^{+0.38}_{-0.22}$ s lasts from surge arrival to completed barrier lift. A dam-like debris pattern stable for more than a short fraction of a second could not be observed.

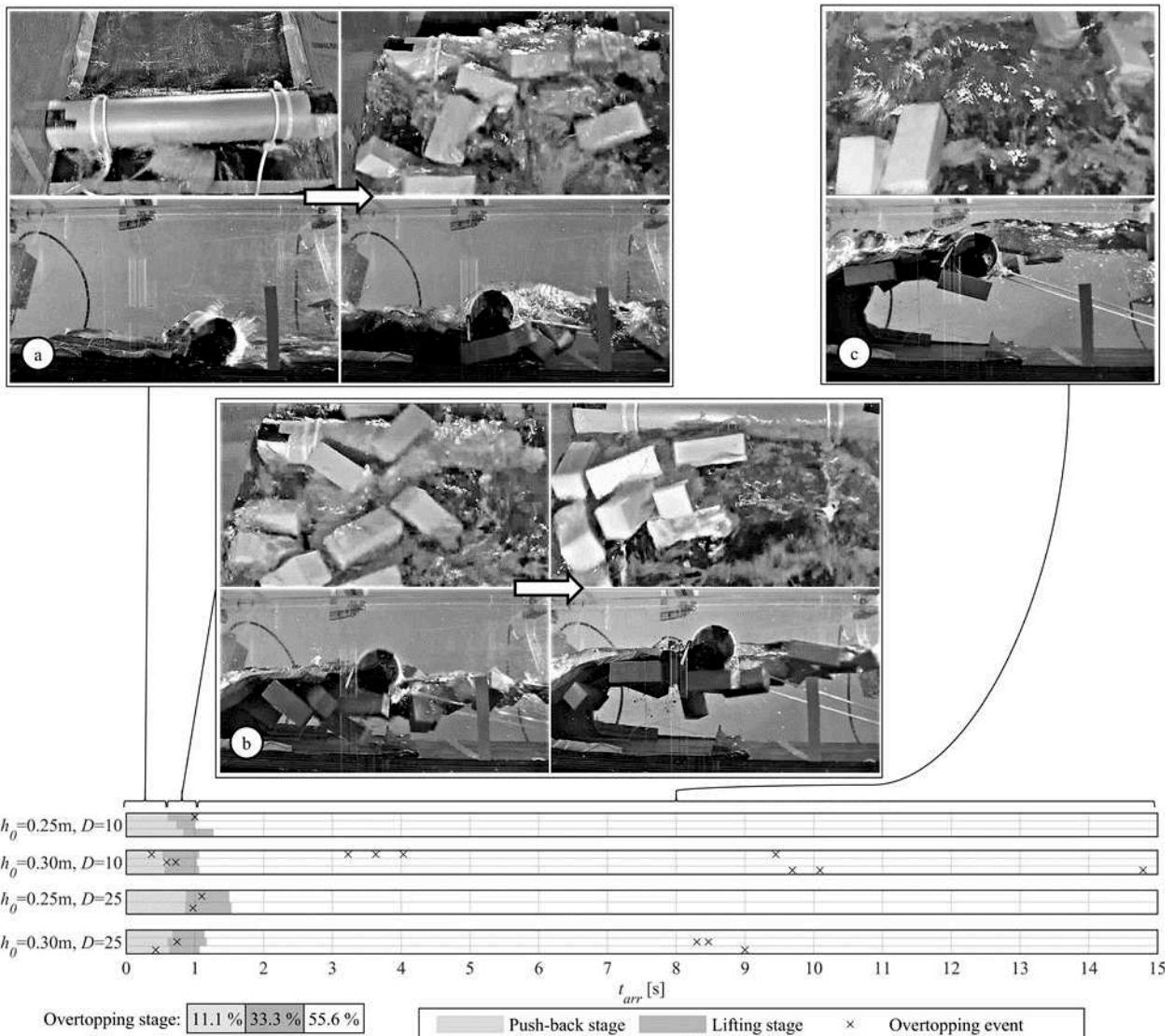


Figure 7: Stages of barrier-debris-interaction recorded by CAM 1 (top in each box) and CAM 2 (bottom in each box) as well as distribution of overtopping events after surge arrival at the SLMB (t_{arr}). The photograph boxes show the interaction process during the (a) *push-back stage*, the (b) *lifting stage* and (c) the *equilibrium state*. Arrows in boxes indicate chronological process from left to right.

3.4 Debris transport mitigation due to SLMB

One objective of this study is to evaluate the SLMB's capability to obstruct tsunami debris transport. The obstruction performance is quantified by the capture efficiency (Stolle et al. 2018b), i.e., the relative amount of debris hindered of moving downstream the barrier. For this purpose, three position modes are introduced to categorize the debris model positions in relation to the barrier (Fig. 8) before the 1st surge reflection arrives at the barrier (see Fig. 3b). Debris models that are washed over the FM of the membrane barrier are categorized as *overtopped*. Whereas the mode *blocked* is attributed with debris found upstream of the FM, the mode *trapped* refers to the cavity that forms when the membrane barrier is lifted (see Fig. 1 and Fig. 8). The decision in which mode a debris is, is made based on the position of its geometric center. Boundaries between mode regions run through the FMs center (Fig. 8).

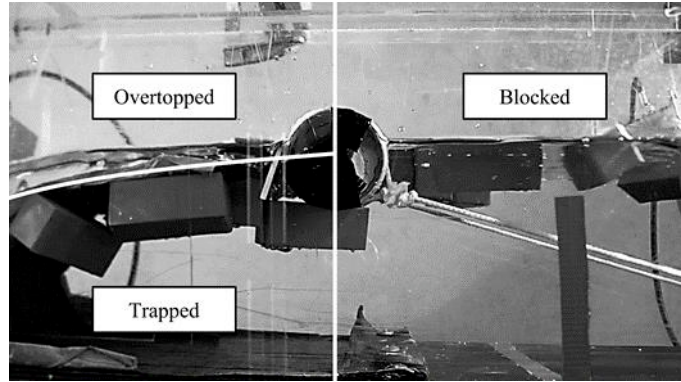


Figure 8: Debris models were categorized based on their position at surge backwash. Models that were moved downstream of the FM are attributed as *overtopped*. Those debris models that were stopped and remained inside the cavity are counted as *trapped*. *Blocked* debris models were stopped and remained upstream of the FM.

Fig. 9 shows the barrier’s performance of capturing debris. Depicted is the distribution of debris in relation to their position mode for different impoundment depths and debris amounts. The dominant mode for each scenario is *blocked*, followed by *trapped* in three out of four scenarios. It is unclear whether the amount of debris governs the mode. This is partly due to the large standard deviations, reaching up to 29% in the high surge impact/low debris loading scenario (see Fig. 9 second stack from left). The capture efficiency can be determined by the combined fraction of debris that are *blocked* or *trapped*. The repetition-averaged percentage of debris that are captured (*blocked* plus *trapped*, see Fig. 9) are 97%, 67%, 96% and 93% (Fig. 9, see (1), (2), (3), (4) respectively). The total average of captured debris is 90% (Fig. 9, see (5)). By considering the large standard deviations, mitigation in the lowest achieving scenario (see Fig. 9, second stack from left) gives a conservative estimation of 51% capture efficiency (Fig. 9, see (6)). Given the number of repetitions is limited to three, some uncertainty remains (number of repetitions is discussed in section 4).

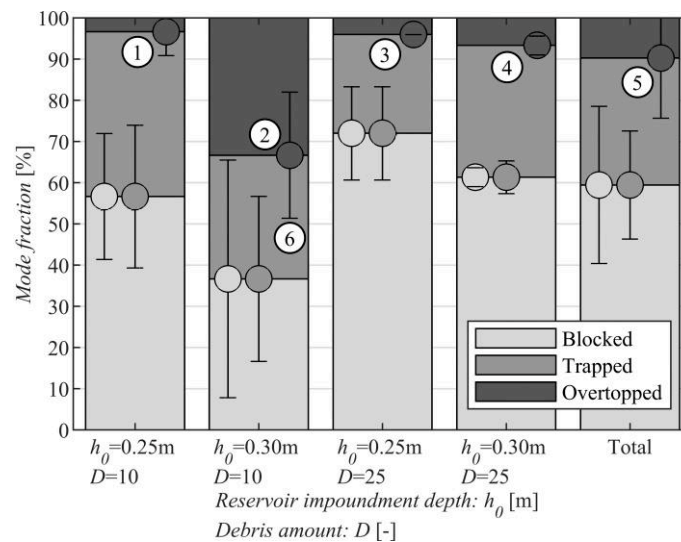


Figure 9: Barrier performance on mitigating debris transport. Error bars show standard deviations within runs.

When upstream flow depths surpassed the barrier height, overtopping was observed (see Fig. 7, box c). In cases where the flow depth over the FM is larger than the debris draft, the debris can pass the barrier. This raises the question if high debris draft lowers the possibility of overtopping and, furthermore, to what extent the capture efficiency is a function of debris geometry and density.

3.5 Scale and model effects

Out of practicability considerations, membrane and cable thickness were not modeled according to scale. It is unclear whether the relatively thick model membrane might lead to high stiffness that in turn could influence barrier behavior. Cables can be scaled only once the forces loading them are known. Since these forces are a priori unknown, unscaled

cables are used in this research. However, tensile stress decreases with increased cable cross-sectional area, which in turn reduces strain. In application, a 40 m long cable could potentially stretch up to 1.2 m if a fracture strain of 3% is applied (Hofland et al. 2015). Reducing strain might also reduce push-back of the FM. This might increase impact forces since horizontal forces cannot result in horizontal movement.

Debris impacting the membrane near the wall slide around the membrane in some cases (Fig. 10b). These debris models were counted as *trapped*. The sealing between flume wall and membrane is disturbed while a debris is passing, leading to leakage which increases downstream flow depth. Furthermore, friction between membrane as well as the FM and the flume wall influences the barriers lifting time.

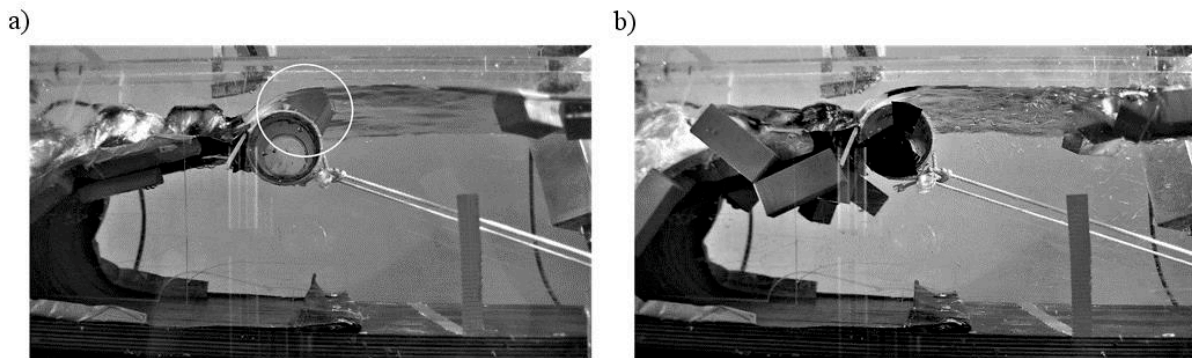


Figure 10: (a) Photographs of near overtopping of a debris model. Debris draft may have an influence on the barrier's capture capability. (b) Demonstration of debris side slipping around the barrier model.

4 Discussion

Instrumentation includes six wave gauges (Fig. 2, Fig. 3c, Table 4). Some wave gauge positions are shifted for the second and third experiment phase (see Fig. 2c). This might limit comparability between phase 1 and the other two phases. However, phases 2 and 3 are comparable with each other. Since all quantitative results are based on data of phase 2 and 3, shifting of WG position does not limit validity of findings.

This study uses broken bores originating from a dam-break mechanism, modelling the hydrodynamic effects of tsunami wave propagating over dry land. In this context, it is noted that the duration of the broken bores when interacting with the SLMB, as well as during the entrainment and transport of debris, is short when compared to observed tsunami durations; these are typically in the range of 5 to 60 min whereas this work utilizes durations of less than 5 min (prototype scale). The issue of appropriate generation of tsunami in laboratory settings is a long-standing topic of debate in the tsunami community (see Goseberg et al. 2013, a review). In the case of debris-SLMB interaction, the duration of the tsunami is however less relevant as the initial phase of the barrier emerging from the ground and its response to the fast rise of the water is the governing process. Were the duration of the flow extended, only less significant changes would occur, and thus, there is little need to find experimental means to obtain longer flow durations.

Interpolation and extrapolation of maximum surface elevation and propagation velocities are carried out linearly since the gradient in surface elevation is approximately constant when no barrier is present (Fig. 4). Interpolations of maximum surface elevation and propagation velocities close to the barrier are not accurate (see Fig. 5). Assuming an even water level downstream the barrier is appropriate for larger distances to the barrier. Close to the barrier, a stilling basin effect is observed (see Fig. 4b, Fig. 5c, d), where a large amount of energy is dissipated in turbulent flow. Thus, the linear interpolation is valid in larger distances downstream the barrier. It has been shown both in numerical and physical studies that tsunami breakwaters and other mitigation systems can lead to energy dissipation (Li et al. 2019; Rahman et al. 2021). The significant reduction in downstream propagation velocity (see Fig. 5c and d) indicates that the SLMB can delay tsunami arrival further inland. This potential advantage of the barrier could be detected by using additional wave gauge and velocimetry probes downstream the barrier in future studies.

The effect of debris on the generation of backwater rise remains unclear from this work, since an increasing flow depth is observed in a high debris loading/low surge impact scenario only. In none of the experimental runs, a significant

increase in maximum flow depths upstream the barrier is detected (Fig. 5a, b, Fig. 6). The lack of backwater rise, as it was observed by Stolle et al. (2017b), could be due to the amount of debris not exceed 25, or the overall blockage ratio within the flume cross section. However, the flow conditions governing the barrier-debris-interaction (Fig. 7) are highly transient, preventing the formation of a debris dam. This is an advantage of such a barrier as additional loads due to debris damming are mitigated. The mentioned benefit together with unimpaired performance under occurrences of overflow represent a strong argument in favor of the SLMB.

Only a single type of debris is used in this study. It is expected that debris types with less draft like boards, hydro poles, beams, or logs more likely pass the barrier. However, 20 ft shipping containers are utilized frequently in previous studies due to their simple geometry and widespread existence in tsunami-prone areas world-wide (Cheng Chen et al. 2020; Derschum et al. 2017; Häfen et al. 2021; Khan et al. 2000; Nouri et al. 2010; Shafiei et al. 2016; Yao et al. 2014; Nistor et al. 2017a). Hence, their usage in this study allows for a high level of comparability with respect to previous studies. Secondly, considering multiple types of debris is beyond the scope of this preliminary study, since a much larger experimental program would be necessary to quantify statistical variations.

As this is a preliminary study, the number of tests for each case was limited to three. This is however within the range of many studies about tsunami debris transport. Repetitions in studies presented in section 1.2 vary from one to six, some of them conducted three tests per case as well (Goseberg et al. 2016a; Goseberg et al. 2016b; Nistor et al. 2017b; Khan et al. 2000; Stolle et al. 2017a; Stolle et al. 2017b; Nouri et al. 2010). Nevertheless, other studies carry out more tests (ten in Yao et al. 2014, ten to thirty in Derschum et al. 2017).

5 Conclusion

This study presents experiments on the interaction between tsunami debris and a SLMB. The onshore propagation of a broken tsunami wave is simulated by dam-break waves run-up on a sloped beach model. Debris models representing 20 ft shipping containers are used. Wave gauge and image data is analyzed. The following conclusions can be drawn from this study:

- Surge propagation velocities upstream the SLMB decrease with increasing debris amount. No effect of debris on maximum flow depths upstream the barrier is identified. Based on these conclusions, impairment of barrier functionality by debris-induced wave parameter alterations is not expected for the type and amount of debris used.
- Transient flow conditions lead to a dynamic barrier-debris-interaction. Rapidly changing positions of debris decrease the potentiality for the formation of a debris dam upstream the SLMB.
- Barrier presence leads to the obstruction of more than half of the debris. Observations suggest that debris properties like draft could affect the obstruction performance. Probability of debris overtopping increases for larger reservoir impoundment depth.

Future research should address statistical validation of the results obtained in this study, as well as application of varying debris characteristics and higher debris loadings.

Acknowledgements

This work was partially funded by start-up funding of Technische Universität Braunschweig provided to Nils Goseberg. The authors are grateful to the constructive and insightful comments voiced by three anonymous reviewers whose comments greatly improved the manuscript.

Author contributions (CRediT)

HS: Conceptualization, Data curation, Formal Analysis, Investigation, Methodology, Software, Validation, Visualization, Writing-original draft. HH: Formal Analysis, Investigation, Resources, Validation, Writing-review & editing. NG: Resources, Supervision, Funding acquisition, Project administration, Writing-review & editing.

Notation

Name	Symbol	Unit
Surge propagation velocity	c	m/s
Debris amount	D	–
Gravitational acceleration	g	m/s ²
Flow depth	h	m
Maximum flow depth	h_{max}	m
Impoundment depth	h_0	m
Time after dam-break	t	s
Time after surge arrival	t_{arr}	s
Gate opening time	t_{op}	s
Distance to dam-break gate	x	m
Maximum surface elevation (maximum flow depth plus beach model height)	η_{max}	m

References

- Ardianti, A.; Mutsuda, H.; Kawawaki, K.; Doi, Y. (2018): Fluid structure interactions between floating debris and tsunami shelter with elastic mooring caused by run-up tsunami. In *Coastal Engineering* 137, pp. 120–132. DOI: 10.1016/j.coastaleng.2018.04.004.
- ASCE (2016): ASCE standard, ASCE/ SEI 7-16, minimum design loads and associated criteria for buildings and other structures.
- Chandramouli, K.; Pannirselvam, N.; Avuthu, S. R.; Anitha, V.; Kumar, M. C. N. (2018): A Study on Tsunami Protection Works. In *International Journal of Engineering Science Invention (IJESI)* (7), pp. 43–46.
- Chanson, H. (2005): Analytical Solution of Dam Break Wave with Flow Resistance: Application to Tsunami Surges. In *XXXI. IAHR Congress, September 12-16, Seoul, Korea* 137, pp. 3341–3356.
- Chanson, H. (2006): Tsunami Surges on Dry Coastal Plains: Application of Dam Break Wave Equations. In *Coastal Engineering Journal* 48 (4), pp. 355–370. DOI: 10.1142/S0578563406001477.
- Cheng Chen; Jun Chen; Peng Lin; Chiwei Chen; Haozhe Chen (2020): Experimental Study of Dam-Break-Like Tsunami Bore Impact Mechanism on a Container Model. In *Polish Maritime Research* 27 (1), pp. 53–59. DOI: 10.2478/pomr-2020-0006.
- Chock, G. Y. K. (2016): Design for Tsunami Loads and Effects in the ASCE 7-16 Standard. In *J. Struct. Eng.* 142 (11), p. 4016093. DOI: 10.1061/(ASCE)ST.1943-541X.0001565.
- Choowong, M.; Murakoshi, N.; Hisada, K.; Charusiri, P.; Charoentitirat, T.; Chutakositkanon, V. et al. (2008): 2004 Indian Ocean tsunami inflow and outflow at Phuket, Thailand. In *Marine Geology* 248 (3-4), pp. 179–192. DOI: 10.1016/j.margeo.2007.10.011.
- Como, Anisa; Mahmoud, Hussam (2013): Numerical evaluation of tsunami debris impact loading on wooden structural walls. In *Engineering Structures* 56, pp. 1249–1261. DOI: 10.1016/j.engstruct.2013.06.023.
- Danielsen, Finn; Sørensen, Mikael K.; Olwig, Mette F.; Selvam, Vaithilingam; Parish, Faizal; Burgess, Neil D. et al. (2005): The Asian tsunami: a protective role for coastal vegetation. In *Science (New York, N.Y.)* 310 (5748), p. 643. DOI: 10.1126/science.1118387.
- Derschum, C.; Stolle, J.; Nistor, I.; Goseberg, N. (2017): Influence Of Wave-Structure Interaction On Tsunami-Driven Debris Impact.

- Dunbar, Paula; McCullough, Heather; Mungov, George; Varner, Jesse; Stroker, Kelly (2011): 2011 Tohoku earthquake and tsunami data available from the National Oceanic and Atmospheric Administration/National Geophysical Data Center. In *Geomatics, Natural Hazards and Risk* 2 (4), pp. 305–323. DOI: 10.1080/19475705.2011.632443.
- EERI (Ed.) (2011): EERI Special Earthquake Report. Learning from Earthquakes. The Japan Tohoku Tsunami of March 11, 2011.
- FEMA (2012): Guidelines for Design of Structures for Vertical Evacuation from Tsunamis FEMA P-646 / April 2012. FEMA P-646, revised Second Edition.
- Fraser, S.; Raby, A.; Pomonis, A.; Goda, K.; Chian, S. C.; Macabuag, J. et al. (2013): Tsunami damage to coastal defences and buildings in the March 11th 2011 M w 9.0 Great East Japan earthquake and tsunami. In *Bull Earthquake Eng* 11 (1), pp. 205–239. DOI: 10.1007/s10518-012-9348-9.
- Goseberg, N.; Nistor, I.; Mikami, T.; Shibayama, T.; Stolle, J. (2016a): Nonintrusive Spatiotemporal Smart Debris Tracking in Turbulent Flows with Application to Debris-Laden Tsunami Inundation. In *J. Hydraul. Eng.* 142 (12), p. 4016058. DOI: 10.1061/(ASCE)HY.1943-7900.0001199.
- Goseberg, N.; Stolle, J.; Nistor, I.; Shibayama, T. (2016b): Experimental analysis of debris motion due the obstruction from fixed obstacles in tsunami-like flow conditions. In *Coastal Engineering* 118, pp. 35–49. DOI: 10.1016/j.coastaleng.2016.08.012.
- Goseberg, N.; Wurpts, A.; Schlurmann, T. (2013): Laboratory-scale generation of tsunami and long waves. In *Coastal Engineering* 79, pp. 57–74. DOI: 10.1016/j.coastaleng.2013.04.006.
- Goseberg, Nils; Schlurmann, Torsten (2015): NON-STATIONARY FLOW AROUND BUILDINGS DURING RUN-UP OF TSUNAMI WAVES ON A PLAIN BEACH. In *Int. Conf. Coastal. Eng.* 1 (34), p. 21. DOI: 10.9753/icce.v34.currents.21.
- Haehnel, R. B.; Daly, S. F. (2004): Maximum Impact Force of Woody Debris on Floodplain Structures. In *J. Hydraul. Eng.* 130 (2), pp. 112–120. DOI: 10.1061/(ASCE)0733-9429(2004)130:3A2(112).
- Häfen, H. von; Goseberg, N.; Stolle, J.; Nistor, I. (2019): Gate-Opening Criteria for Generating Dam-Break Waves. In *J. Hydraul. Eng.* 145 (3), p. 4019002. DOI: 10.1061/(ASCE)HY.1943-7900.0001567.
- Häfen, Hajo von; Stolle, Jacob; Nistor, Ioan; Goseberg, Nils (2021): Side-by-side entrainment and displacement of cuboids due to a tsunami-like wave. In *Coastal Engineering* 164, p. 103819. DOI: 10.1016/j.coastaleng.2020.103819.
- Harbitz, C. B.; Nakamura, Y.; Arikawa, T.; Baykal, C.; Dogan, G. G.; Frauenfelder, R. et al. (2016): Risk Assessment and Design of Prevention Structures for Enhanced Tsunami Disaster Resilience (RAPSODI)/Euro-Japan Collaboration. In *Coastal Engineering Journal* 58 (4), 1640012-1-1640012-37. DOI: 10.1142/S057856341640012X.
- Hofland, B.; Marissen, R.; Bergsma, O. (2015): Dynamic behaviour of a flexible membrane tsunami Barrier with Dyneema. Proc. Coastal Structures and Solutions to Coastal Disasters Joint Conference. 9 - 11 September 2015. Pages 235 - 245
- Jaffe, Bruce E.; Gelfenbuam, Guy (2007): A simple model for calculating tsunami flow speed from tsunami deposits. In *Sedimentary Geology* 200 (3-4), pp. 347–361. DOI: 10.1016/j.sedgeo.2007.01.013.
- Kato, F.; Suwa, Y.; Watanabe, K.; Hatogai, S. (2012): Mechanisms of Coastal Dike Failure induced by the Great East Japan Earthquake Tsunami. In *Int. Conf. Coastal. Eng.* 1 (33), p. 40. DOI: 10.9753/icce.v33.structures.40.
- Kawata, Y.; Benson, B. C.; Borrero, J. C.; Borrero, J. L.; Davies, H. L.; Lange, W. P. de et al. (1999): Tsunami in Papua New Guinea was as intense as first thought. In *Eos Trans. AGU* 80 (9), p. 101. DOI: 10.1029/99EO00065.
- Khan, Ab. A.; Steffler, P. M.; Gerard, R. (2000): Dam-Break Surges with Floating Debris. In *J. Hydraul. Eng.* 126 (5), pp. 375–379. DOI: 10.1061/(ASCE)0733-9429(2000)126:3A5(375).
- Kimura, Y.; Mase, H.; Nakayasu, K.; Morii, T. (2014): Experimental Study on Real-Time Tsunami Protection Structures. In *J. Waterway, Port, Coastal, Ocean Eng.* 140 (3), p. 4014003. DOI: 10.1061/(ASCE)WW.1943-5460.0000218.
- Ko, H. T.-S.; Cox, D. T.; Riggs, H. R.; Naito, C. J. (2015): Hydraulic Experiments on Impact Forces from Tsunami-Driven Debris. In *J. Waterway, Port, Coastal, Ocean Eng.* 141 (3), p. 4014043. DOI: 10.1061/(ASCE)WW.1943-5460.0000286.

- Lange, S. I. de; Santa, N.; Pudasaini, S. P.; Kleinhans, M. G.; Haas, T. de (2020): Debris-flow generated tsunamis and their dependence on debris-flow dynamics. In *Coastal Engineering* 157 (5088), p. 103623. DOI: 10.1016/j.coastaleng.2019.103623.
- Lauber, G.; Hager, W. H. (1998): Experiments to dambreak wave: Horizontal channel. In *Journal of Hydraulic Research* 36 (3), pp. 291–307. DOI: 10.1080/00221689809498620.
- Lawrence, Sean; Nandasena, N. A. K. (2019): Hybrid Approach for Tsunami Protection: Effect of Embankment-type Seawall and Vegetation on Tsunami Reduction. In *KSCE J Civ Eng* 23 (6), pp. 2391–2396. DOI: 10.1007/s12205-019-1759-6.
- Li, Y. L.; Ma, Y.; Deng, R.; Jiang, D. P.; Hu, Z. (2019): Research on dam-break induced tsunami bore acting on the triangular breakwater based on high order 3D CLSVOF-THINC/WLIC-IBM approaching. In *Ocean Engineering* 182, pp. 645–659. DOI: 10.1016/j.oceaneng.2019.03.067.
- Marissen, R. (2011): Design with Ultra Strong Polyethylene Fibers. In *MSA* 02 (05), pp. 319–330. DOI: 10.4236/msa.2011.25042.
- Marissen, R.; Mulder, J. S.; Wienke, D.; Bergsma, O. (2013): Design Considerations on a Flexible Membrane Tsunami Flood Barrier. In *MSA* 04 (12), pp. 846–855. DOI: 10.4236/msa.2013.412108.
- Matsutomi, Hideo (2009): Method for Estimating Collision Force of Driftwood Accompanying Tsunami Inundation Flow. In *J. Disaster Res.* 4 (6), pp. 435–440. DOI: 10.20965/jdr.2009.p0435.
- Melville, Bruce W.; Dongol, D. M. (1992): Bridge Pier Scour with Debris Accumulation. In *J. Hydraul. Eng.* 118 (9), pp. 1306–1310. DOI: 10.1061/(ASCE)0733-9429(1992)118:9(1306).
- Morton, R. A.; Gelfenbaum, G.; Jaffe, B. E. (2007): Physical criteria for distinguishing sandy tsunami and storm deposits using modern examples. In *Sedimentary Geology* 200 (3-4), pp. 184–207. DOI: 10.1016/j.sedgeo.2007.01.003.
- Naito, C.; Cercone, C.; Riggs, H. R.; Cox, D. (2014): Procedure for Site Assessment of the Potential for Tsunami Debris Impact. In *J. Waterway, Port, Coastal, Ocean Eng.* 140 (2), pp. 223–232. DOI: 10.1061/(ASCE)WW.1943-5460.0000222.
- Nistor, I.; Goseberg, N.; Stolle, J. (2017a): Tsunami-Driven Debris Motion and Loads: A Critical Review. In *Front. Built Environ.* 3, p. 7057. DOI: 10.3389/fbuil.2017.00002.
- Nistor, I.; Goseberg, N.; Stolle, J.; Mikami, T.; Shibayama, T.; Nakamura, R.; Matsuba, S. (2017b): Experimental Investigations of Debris Dynamics over a Horizontal Plane. In *J. Waterway, Port, Coastal, Ocean Eng.* 143 (3), p. 4016022. DOI: 10.1061/(ASCE)WW.1943-5460.0000371.
- Nistor, I.; Palermo, D.; Nouri, Y.; Murty, T.; Saatcioglu, M. (2009): Tsunami-Induced Forces on Structures, pp. 261–286. DOI: 10.1142/9789812819307_0011.
- Nouri, Y.; Nistor, I.; Palermo, D.; Cornett, A. (2010): Experimental Investigation of Tsunami Impact on Free Standing Structures. In *Coastal Engineering Journal* 52 (1), pp. 43–70. DOI: 10.1142/S0578563410002117.
- Paczkowski, K.; Riggs, H. R.; Naito, C. J.; Lehmann, A. (2012): A one-dimensional model for impact forces resulting from high mass, low velocity debris. In *Structural Engineering and Mechanics* 42 (6), pp. 831–847. DOI: 10.12989/sem.2012.42.6.831.
- Pagliara, Stefano; Carnacina, Iacopo (2013): Bridge pier flow field in the presence of debris accumulation. In *Proceedings of the Institution of Civil Engineers - Water Management* 166 (4), pp. 187–198. DOI: 10.1680/wama.11.00060.
- Palermo, Dan; Nistor, Ioan; Saatcioglu, Murat; Ghobarah, Ahmed (2013): Impact and damage to structures during the 27 February 2010 Chile tsunami. In *Can. J. Civ. Eng.* 40 (8), pp. 750–758. DOI: 10.1139/cjce-2012-0553.
- Pasha, Ghufuran Ahmed; Tanaka, Norio (2016): Effectiveness of Finite Length Inland Forest in Trapping Tsunami-Borne Wood Debris. In *J. Earthquake and Tsunami* 10 (04), p. 1650008. DOI: 10.1142/S1793431116500081.
- Pethick, J. (1984): An introduction to coastal geomorphology. London: Arnold.
- Rahman, Md Abedur; Tanaka, Norio; Rashedunnabi, A. H. M. (2021): Flume Experiments on Flow Analysis and Energy Reduction through a Compound Tsunami Mitigation System with a Seaward Embankment and Landward Vegetation over a Mound. In *Geosciences* 11 (2), p. 90. DOI: 10.3390/geosciences11020090.
- Ritter, A. (1892): Die Fortpflanzung der Wasserwellen. In *Verein Deutscher Ingenieure (Zeitschrift 36)*, pp. 947–954.

- Robertson, Ian N.; Riggs, H. Ronald; Yim, Solomon C.; Young, Yin Lu (2007): Lessons from Hurricane Katrina Storm Surge on Bridges and Buildings. In *J. Waterway, Port, Coastal, Ocean Eng.* 133 (6), pp. 463–483. DOI: 10.1061/(ASCE)0733-950X(2007)133:6(463).
- ROH (2018): City and County of Honolulu Building Code. Available online at <https://www.honolulu.gov/cms-ocs-menu/site-ocs-sitearticles/972-roh-chapter-16-1.html>, checked on 9/28/2018.
- Schmocker, Lukas; Hager, Willi H. (2011): Probability of Drift Blockage at Bridge Decks. In *J. Hydraul. Eng.* 137 (4), pp. 470–479. DOI: 10.1061/(ASCE)HY.1943-7900.0000319.
- Norm ISO 668:2013(E), 8/1/2013: Series 1 freight containers - Classification, dimensions and ratings.
- Shafiei, S.; Melville, B. W.; Shamseldin, A. Y.; Beskhyroun, S.; Adams, K. N. (2016): Measurements of tsunami-borne debris impact on structures using an embedded accelerometer. In *Journal of Hydraulic Research* 54 (4), pp. 435–449. DOI: 10.1080/00221686.2016.1170071.
- Shao, Songdong (2005): SPH simulation of solitary wave interaction with a curtain-type breakwater. In *Journal of Hydraulic Research* 43 (4), pp. 366–375. DOI: 10.1080/00221680509500132.
- Shibayama, T. (2015): 2004 Indian Ocean Tsunami. In Hiroshi Takagi, Miguel Esteban, Tomoya Shibayama (Eds.): Handbook of coastal disaster mitigation for engineers and planners. First edition. Amsterdam: Elsevier, pp. 3–19.
- Shuto, Nobuo; Fujima, Koji (2009): A short history of tsunami research and countermeasures in Japan. In *Proceedings of the Japan Academy. Series B, Physical and biological sciences* 85 (8), pp. 267–275. DOI: 10.2183/pjab.85.267.
- Stolle, J.; Goseberg, N.; Nistor, I.; Petriu, E. (2018a): Probabilistic Investigation and Risk Assessment of Debris Transport in Extreme Hydrodynamic Conditions. In *J. Waterway, Port, Coastal, Ocean Eng.* 144 (1), p. 4017039. DOI: 10.1061/(ASCE)WW.1943-5460.0000428.
- Stolle, J.; Nistor, I.; Goseberg, N.; Mikami, T.; Shibayama, T. (2017a): Entrainment and Transport Dynamics of Shipping Containers in Extreme Hydrodynamic Conditions. In *Coastal Engineering Journal* 59 (3), 1750011-1-1750011-30. DOI: 10.1142/S0578563417500115.
- Stolle, J.; Takabatake, T.; Mikami, T.; Shibayama, T.; Goseberg, N.; Nistor, I.; Petriu, E. (2017b): Experimental Investigation of Debris-Induced Loading in Tsunami-Like Flood Events. In *Geosciences* 7 (3), p. 74. DOI: 10.3390/geosciences7030074.
- Stolle, Jacob; Takabatake, Tomoyuki; Nistor, Ioan; Mikami, Takahito; Nishizaki, Shinsaku; Hamano, Go et al. (2018b): Experimental investigation of debris damming loads under transient supercritical flow conditions. In *Coastal Engineering* 139, pp. 16–31. DOI: 10.1016/j.coastaleng.2018.04.026.
- Strusińska-Correia, Agnieszka (2017): Tsunami mitigation in Japan after the 2011 Tōhoku Tsunami. In *International Journal of Disaster Risk Reduction* 22, pp. 397–411. DOI: 10.1016/j.ijdrr.2017.02.001.
- Takagi, Hiroshi; Bricker, Jeremy d. (2014): Assessment of the Effectiveness of General Breakwaters in Reducing Tsunami Inundation in Ishinomaki. In *Coastal Engineering Journal* 56 (4), 1450018-1-1450018-21. DOI: 10.1142/S0578563414500181.
- Takahashi, S.; Kuriyama, Y.; Tomita, T.; Kawai, Y.; Arikawa, T.; Tatsumi, D. (2011): Urgent survey for 2011 great east japan earthquake and tsunami disaster in ports and coasts - part I (Tsunami). In *PARI Technical Note 1231*. Available online at <https://www.weather.gov/media/ctwp/PDF/Tohokutsunamiportssurvey.pdf>.
- Tanaka, Norio (2009): Vegetation bioshields for tsunami mitigation: review of effectiveness, limitations, construction, and sustainable management. In *Landscape Ecol Eng* 5 (1), pp. 71–79. DOI: 10.1007/s11355-008-0058-z.
- Tanaka, Norio; Sasaki, Yasushi; Mowjood, M. I. M.; Jinadasa, K. B. S. N.; Homchuen, Samang (2007): Coastal vegetation structures and their functions in tsunami protection: experience of the recent Indian Ocean tsunami. In *Landscape Ecol Eng* 3 (1), pp. 33–45. DOI: 10.1007/s11355-006-0013-9.
- Tomiczek, Tori; Wargula, Anna; Lomónaco, Pedro; Goodwin, Sabella; Cox, Dan; Kennedy, Andrew; Lynett, Pat (2020): Physical model investigation of mid-scale mangrove effects on flow hydrodynamics and pressures and loads in the built environment. In *Coastal Engineering* 162, p. 103791. DOI: 10.1016/j.coastaleng.2020.103791.
- Umeda, Shinya; Saitoh, Takehisa; Furumichi, Hiroko (2018): Mitigation effects of onshore perforated barriers on inundation and forces induced by tsunami and tsunami-driven objects. In *Ocean Engineering* 152, pp. 89–99. DOI: 10.1016/j.oceaneng.2018.01.051.
- Whitham, G. B. (1955): The effects of hydraulic resistance in the dam-break problem. In *Proc. R. Soc. Lond. A* 227 (1170), pp. 399–407. DOI: 10.1098/rspa.1955.0019.

- Widiyanto, W.; Santoso, P. B.; Hsiao, S.; Imananta, R. T. (2019): Post-event Field Survey of 28 September 2018 Sulawesi Earthquake and Tsunami. In *Nat. Hazards Earth Syst. Sci. Discuss.*, pp. 1–23. DOI: 10.5194/nhess-2019-91.
- Yamazaki, Yoshiki; Cheung, Kwok Fai (2011): Shelf resonance and impact of near-field tsunami generated by the 2010 Chile earthquake. In *Geophys. Res. Lett.* 38 (12), n/a-n/a. DOI: 10.1029/2011GL047508.
- Yao, Y.; Huang, Z.; Lo, E. Y. M.; Shen, H. (2014): A Preliminary Laboratory Study of Motion of Floating Debris Generated by Solitary Waves Running up a Beach. In *J. Earthquake and Tsunami* 08 (03), p. 1440006. DOI: 10.1142/S1793431114400065.